

Electronic Control of the Position of the Pb Atom on the Surface of B₈ Borozene in the PbB₈ Cluster

Published as part of *The Journal of Physical Chemistry A* virtual special issue “Xueming Yang Festschrift”.

Wei-Jia Chen,[§] Hyun Wook Choi,[§] Joseph Cavanagh, Dao-Fu Yuan,^{*} and Lai-Sheng Wang^{*}



Cite This: *J. Phys. Chem. A* 2024, 128, 3564–3570



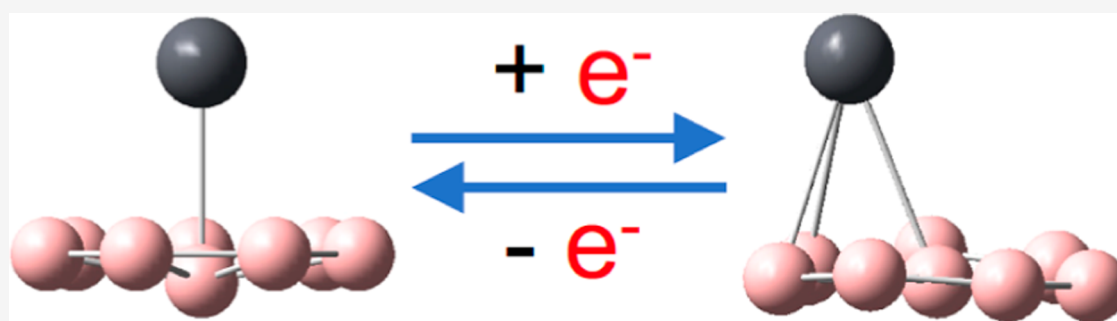
Read Online

ACCESS |

Metrics & More

Article Recommendations

Supporting Information



ABSTRACT: Spontaneous symmetry-breaking is common in chemical and physical systems. Here, we show that by adding an electron to the C_{7v} PbB_8 cluster, which consists of a planar B_8 disk with the Pb atom situated along the C_7 axis, the Pb atom spontaneously moves to the off-axis position in the PbB_8^- anion. Photoelectron spectroscopy of PbB_8^- reveals a broad ground-state transition and a large energy gap, suggesting a highly stable closed-shell PbB_8 borozene complex and a significant geometry change upon electron detachment. Quantum chemistry calculations indicate that the lowest unoccupied molecular orbital of the C_{7v} PbB_8 cluster is a degenerate π orbital mainly consisting of the Pb $6p_x$ and $6p_y$ atomic orbitals. Occupation of one of the $6p$ orbitals spontaneously break the C_{7v} symmetry in the anion due to the Jahn–Teller effect. The large amplitude of the position change of Pb in PbB_8^- relative to PbB_8 is surprising owing to bonding interactions between the Pb $6p$ orbital with the π orbital of the B_8 borozene.

1. INTRODUCTION

Spontaneous symmetry breaking is ubiquitous in chemical and physical systems due to the Jahn–Teller (JT) effect, which occurs for degenerate electronic states.¹ Molecular symmetries can be likewise restored when the underlying degeneracy is removed, which can often be accomplished by the removal or addition of an electron. The JT effect is widely observed in electronic spectroscopy, and the symmetry breaking can be subtle or minor. For molecules involving heavy elements, strong spin–orbit couplings can even suppress the JT effect. Here, we report the observation of an extraordinarily pronounced JT distortion in the PbB_8^- anionic cluster, where a large change of the position of the heavy Pb atom is found on the surface of the planar B_8 boron disk upon the addition of an electron to the highly symmetric C_{7v} PbB_8 cluster.

Boron is an electron-deficient element with complicated chemical bonding and structures. The electron deficiency of boron leads to electron sharing and delocalization in borane compounds and bulk boron allotropes.^{2–4} During the past two decades, the structures and bonding of size-selected boron clusters have been elucidated via combined experimental and theoretical investigations.^{5–10} Different from bulk boron

materials, finite boron clusters have been found to have two-dimensional (2D) structures consisting of B_3 triangles, decorated with tetragonal, pentagonal, or hexagonal holes. The discovery of the planar B_{36} cluster with a central hexagonal hole provides the first experimental evidence of the viability of 2D boron nanostructures, named borophenes,^{11,12} which have been synthesized on inert substrates.^{13,14} The B_7^- , B_8^- , and B_9^- clusters were among the first few boron clusters to be investigated by joint photoelectron spectroscopy (PES) and theoretical calculations and they were all found to possess 2D structures with a central B atom inside a B_n ring.^{15,16} Recently, the B_7^{3-} , B_8^{2-} , and B_9^- series of closed-shell species are shown to possess similar π bonding akin to that in $C_3H_5^-$, C_6H_6 , and $C_7H_7^+$, respectively, and a name “borozene” is coined to highlight their analogy to the classical aromatic hydrocarbon

Received: February 27, 2024

Revised: April 15, 2024

Accepted: April 18, 2024

Published: April 27, 2024



molecules.¹⁷ Among the borozenes, the D_{7h} B_8^{2-} is unique for its high stability originated from both its double aromaticity and the fact that the B_7 ring has the perfect size to host a central B atom. The B_8^{2-} borozene has been realized experimentally in a variety of MB_8 and M_2B_8 complexes^{18–23} and predicted to exist in many more MB_8 systems.^{24–32} It has been recently found that Au and Bi tend to be bonded to the edge of the B_8^{2-} borozene,^{21,22} whereas transition metals (TMs) have been known previously to form $TM@B_8$ -type borometallic molecular wheels with the TM atom located in the center of a B_8 ring,^{33–42} rather than the MB_8 borozene complexes.

In the current article, we present an investigation of a heavy p-block metal borozene complex, PbB_8 . PES of the PbB_8^- anionic cluster reveals a large energy gap and a broad ground-state detachment transition, implying a highly stable PbB_8 neutral cluster and a large geometry change from the anion to the neutral ground state. Theoretical calculations show that the PbB_8^- anion has C_s symmetry with a $^2A'$ electronic state, in which the Pb atom is bonded to a B_3 triangle above the B_8 disk framework, whereas the neutral PbB_8 is a highly symmetric closed-shell C_{7v} borozene complex [$Pb^{2+}(B_8^{2-})$] with the Pb atom on the C_7 axis. The symmetry breaking in the anion is due to the JT effect as a result of the occupation of the degenerate e_1 lowest unoccupied molecular orbital (LUMO) of PbB_8 by the extra electron. While the B_8 framework does not undergo significant geometry changes, the position of the Pb atom is moved substantially off the C_7 axis in the anion due to bonding interactions between the Pb 6p orbital and the borozene π orbital.

2. EXPERIMENTAL AND THEORETICAL METHODS

2.1. Photoelectron Spectroscopy. The experiment was conducted using a magnetic bottle PES apparatus equipped with a laser-vaporization supersonic cluster source.⁸ The PbB_8^- clusters were produced by laser vaporization of a disk target made of Pb- and ^{10}B -enriched boron powders. The laser-induced plasma off the target surface was quenched by a high-pressure helium carrier gas seeded with 5% argon. Clusters formed inside the nozzle were entrained by the carrier gas and underwent a supersonic expansion. After passing a skimmer, negatively charged clusters in the collimated molecular beam were extracted at 90° into a time-of-flight mass analyzer. The PbB_8^- cluster was selected by a mass gate and decelerated before crossing a detachment laser. Two detachment laser wavelengths were employed in the current work, 532 nm (2.331 eV) and 266 nm (4.661 eV) from an Nd/YAG laser. Photoelectrons were collected by the magnetic bottle and analyzed in a 3.5 m-long electron time-of-flight tube. Photoelectron kinetic energies were calibrated with the known transitions of the Pb^- atomic anion. The electron kinetic energy (E_k) resolution ($\Delta E_k/E_k$) of the magnetic bottle analyzer was approximately 2.5%, i.e., about 25 meV for 1 eV electrons.

2.2. Theoretical Method. Theoretical calculations were performed to understand the structures and bonding properties of the $PbB_8^{-/0}$ clusters using the Gaussian 09 program.⁴⁵ Since the PbB_8^- cluster is isoelectronic to the BiB_8 neutral cluster, their global minimum (GM) structures are expected to be similar to each other. Building on our previous findings on $BiB_8^{-/0}$,²² we utilized the GM structure and the three low-lying isomers of BiB_8 to help identify the GM structure of the PbB_8^- cluster. Both doublet and quartet spin multiplicities were

tested for PbB_8^- at the level of PBE0/LANL2DZ. The low-lying isomers were reoptimized at the PBE0 level using the aug-cc-pVTZ basis set for the B atoms and the aug-cc-pVTZ-pp basis set with the relativistic pseudopotentials (ECP60MDF) for the Pb atom.^{44–46} For the GM structure, the adiabatic detachment energy (ADE) was calculated as the difference in energy between the optimized anion and the optimized neutral structure. The first vertical detachment energy (VDE₁) was calculated as the difference in energy between the optimized anion and the neutral at the optimized structure of the anion. Higher VDEs were calculated using time-dependent density functional theory at the PBE0/aug-cc-pVTZ level of theory at the anion structure.^{47,48} Though we did not explicitly account for the spin–orbit coupling effects, our calculated detachment energies are found to agree well with the experimental results.

Chemical bonding analyses were performed using the adaptive natural density partitioning (AdNDP) method developed by the Boldyrev group,^{49,50} as implemented in Multiwfn.⁵¹ The AdNDP method relies on the electron pair as the fundamental component of chemical bonding models, characterizing the electronic structure in the context of n -center two-electrons (nc - $2e$) bonds. The AdNDP approach serves as an extension of the natural bonding orbital analysis and is based on the concept of occupation numbers (ONs). In this context, the closer an ON for a specific bond approaches 2.0 (or 1.0 for single-electron bonds), the more dependable the bonding representation becomes.

3. RESULTS

3.1. Experimental Results. The photoelectron spectra of PbB_8^- are shown in Figure 1 at two photon energies. Detachment features are denoted by letters, where X indicates the detachment transition from the ground state of the anion to that of the neutral. The bands labeled from A to C represent detachment transitions from the ground state of the anion to

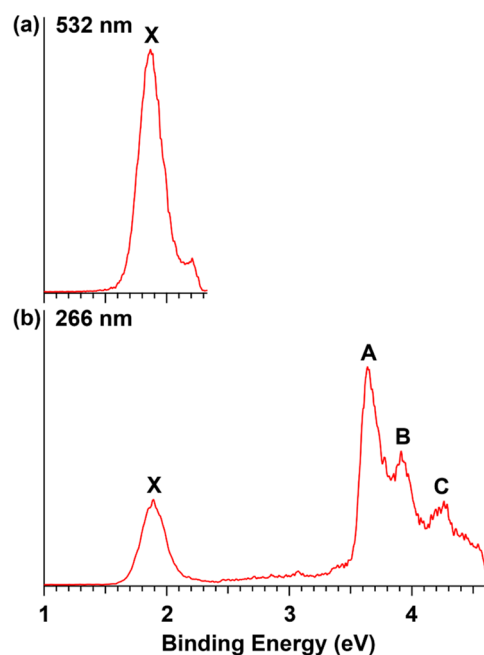


Figure 1. Photoelectron spectra of PbB_8^- at (a) 532 nm (2.331 eV) and (b) 266 nm (4.661 eV).

excited states of the neutral final states. The photoelectron spectrum of PbB_8^- at 532 nm (Figure 1a) displays one broad band X centered at 1.87 eV, which defines the VDE to the neutral ground electronic state. The ADE is estimated to be 1.64 eV from the onset of band X. The 266 nm spectrum (Figure 1b) reveals a large energy gap between band X and the next major detachment band A at a VDE of 3.64 eV. A close-by band B is observed at 3.91 eV. The weak band C at 4.26 eV is broad, and there seems to be unresolved features on the higher binding energy side of band C. All the observed VDEs are given in Table 1, where they are compared with the theoretical results.

Table 1. Experimental VDEs of PbB_8^- in Comparison with the Calculated Values at the PBE0/aug-cc-pVTZ Level of Theory for the GM C_s ($^2A'$) Structure^b

band	VDE (exp.) ^a	final state and electron configuration	VDE (theo.) ^a
X	1.87	$^1A'$ {...0.19a ² 20a ² 11a ² 21a ⁰ }	1.69
A	3.64	$^3A''$ {...0.19a ² 20a ² 11a ¹ 21a ¹ }	3.55
B	3.91	$^3A'$ {...0.19a ² 20a ¹ 11a ² 21a ¹ }	3.77
C	4.26	$^1A''$ {...0.19a ² 20a ² 11a ¹ 21a ¹ }	4.03
		$^1A'$ {...0.19a ² 20a ¹ 11a ² 21a ¹ }	4.16

^aThe observed electron detachment threshold was 1.64 eV, and the computed ADE is 0.93 eV. ^bAll energies are in eV.

3.2. Theoretical Results. The GM and the low-lying isomer are shown in Figure 2 for both the anion and the

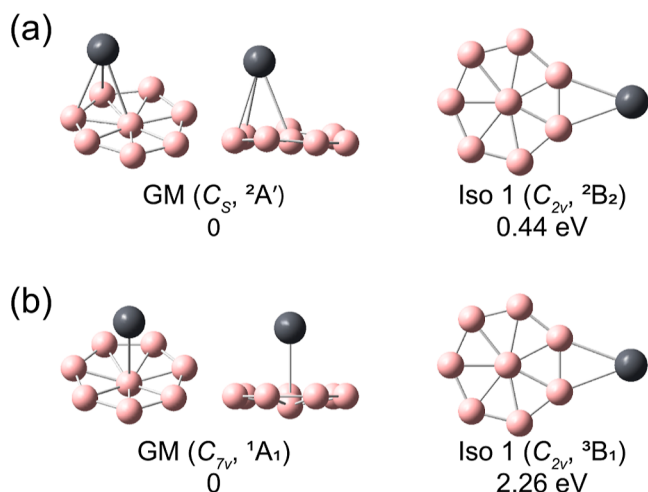


Figure 2. GM and low-lying isomer of (a) PbB_8^- and (b) PbB_8 . Relative energies are given in eV at the PBE0/aug-cc-pVTZ level. The coordinates of these structures are given in Tables S2–S5.

neutral. The GM of PbB_8^- has C_s symmetry with a $^2A'$ electronic state, which consists of a B_8 disk with the Pb atom located above one of the B_3 triangles. Iso1 of PbB_8^- features a Pb atom bonded to the edge of the B_8 disk, which is 0.44 eV above the GM structure. Both the GM and Iso1 of PbB_8^- are similar to those of the isoelectronic BiB_8 cluster.²² The GM structure of neutral PbB_8 is a closed shell and has a high symmetry C_{7v} structure with a large change of the Pb position in comparison with the GM of the anion. Iso1 of PbB_8 (C_{2v} , 3B_1) is similar to that of the anion, but it is 2.26 eV higher in energy than the GM, indicating the overwhelming stability of the C_{7v} structure for PbB_8 . The theoretical ADE and VDEs for

the GM of PbB_8^- are compared with the experimental data in Table 1 and Figure S1. The computed ADE and VDEs for Iso1 of PbB_8^- are given in Table S1.

4. DISCUSSION

4.1. Comparison between Experiment and Theory.

The valence molecular orbitals (MOs) for the C_s GM of PbB_8^- are given in Figure 3. The first PES band X corresponds to electron detachment from the singly occupied MO (SOMO, $21a'$). The calculated VDE₁ of 1.69 eV is in good agreement with the experimental result of 1.87 eV (Table 1). However, the calculated ADE of 0.93 eV is significantly smaller than the estimated experimental value of 1.64 eV from the onset of band X (Figure 1). This is due to the huge geometry change between the anion and the neutral ground state, such that there is a negligible Franck–Condon (FC) factor for the 0–0 transition. This is confirmed by the computed FC factors in comparison with the experimental data, as presented in Figure S2. The computed FC profile shows that the most active vibrational mode is the rocking mode of the B_8 disk around the Pb atom, in agreement with the large change of the position of the Pb atom from the anion to the neutral ground state (Figure 2). The rocking mode is the lowest frequency vibrational mode of PbB_8 with a computed frequency of 168 cm^{-1} at the PBE0 level. The maximum FC factor corresponds to $\nu = 26$ of the rocking vibrational mode of PbB_8 (Figure S2). The excitation energy of $\nu = 26$ (0.54 eV) should define approximately the energy separation between the ADE and VDE of band X. Therefore, according to the FC calculation, the ADE of PbB_8^- should be ~ 1.33 eV, where the FC factor is negligible. In cases where there are large geometry changes from the anion to the neutral, the ADEs cannot be measured from PES. A similar example was reported recently for SO_3^- , which has a pyramidal structure (C_{3v}), while neutral SO_3 is planar (D_{3h}).⁵² The photoelectron spectra of SO_3^- display a broad vibrational progression in the umbrella mode, and there is a negligible FC factor for the 0–0 transition.

The detachment from the full highest occupied MO (HOMO, $11a''$) results in a high-spin ($^3A''$) and a low-spin ($^1A''$) final state. The computed VDE of 3.55 eV for the triplet final state is in good agreement with the experimental VDE of band A (Table 1). In particular, the large energy gap between bands X and A is well reproduced by the theoretical data. The theoretical VDE of 4.03 eV for the singlet final state should correspond to band C at 4.26 eV. Detachment from the HOMO – 1 ($20a'$) produces both a $^3A'$ triplet and a $^1A'$ singlet neutral state. The calculated VDE for the $^3A'$ final state of 3.77 eV agrees well with band B at 3.91 eV, whereas that for the $^1A'$ final state (4.16 eV) likely corresponds to the weak unidentified signals beyond band C (Figure S1). Overall, the theoretical results for the GM of PbB_8^- are in excellent agreement with the experimental observations, unequivocally confirming the C_s GM structure. We also calculated the detachment energies for Iso1 (Table S1), which completely disagree with the major PES features. We note that the computed VDEs for Iso1 of PbB_8^- may correspond to the very weak signals observed between bands A and B (Figure S3), suggesting that Iso1 might be very weakly populated. This observation is consistent with the C_s GM of PbB_8^- .

4.2. Chemical Bonding in PbB_8 and the Origin of the Large Geometry Change in the PbB_8^- Anion. The chemical bonding in the PbB_8 cluster can be understood better using the AdNDP analysis, as shown in Figure 4, which

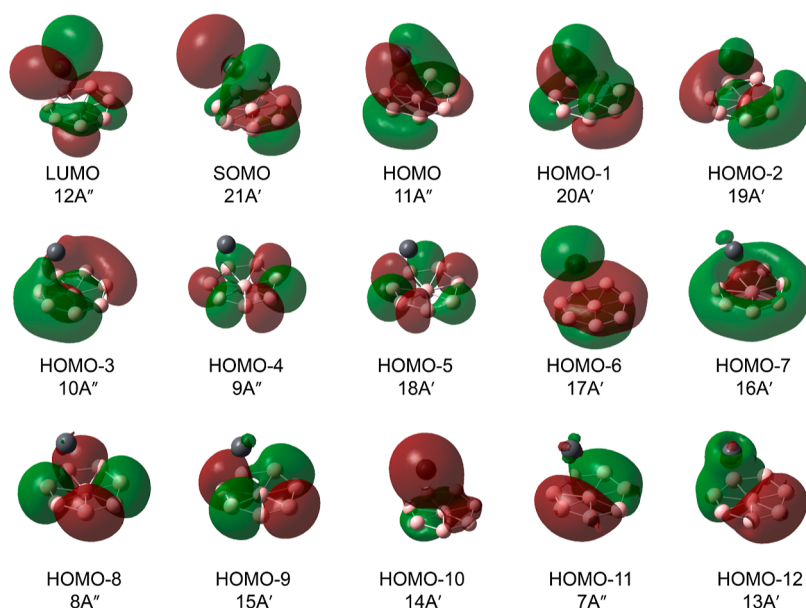


Figure 3. Valence MOs for the C_s GM of PbB_8^- .

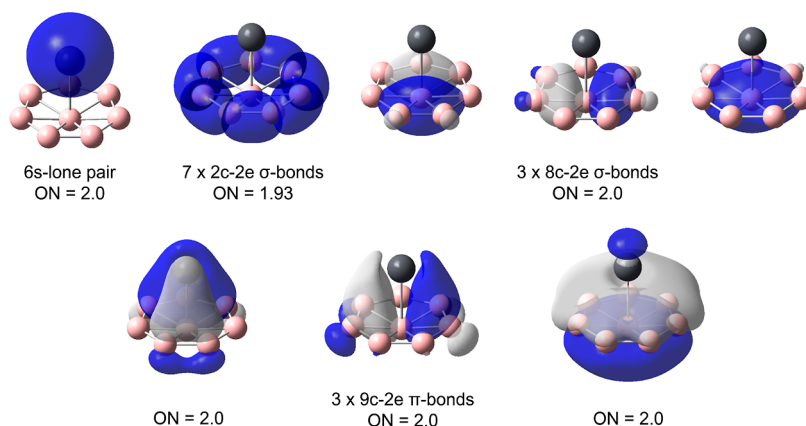


Figure 4. AdNDP bonding analysis for the GM structure of PbB_8 . ON stands for ON.

reveals a 6s lone pair on Pb, seven two-center two-electron (2c-2e) B–B σ bonds on the periphery of the B_8 motif, three 8c-2e σ bonds, and three 9c-2e π bonds. The 6s electrons on Pb are relatively inert due to the strong relativistic effects,⁵³ and Pb acts as a valence 2+ element. Thus, the closed-shell PbB_8 cluster is a perfect $Pb^{2+}(B_8^{2-})$ borozene complex, where there are also clear covalent interactions between the Pb 6p orbitals with the π orbitals on the B_8 motif (Figure 4).

The valence MOs shown in Figure 5 provide further insight into the chemical bonding in the PbB_8 borozene complex and the large geometry change upon addition of an electron in the PbB_8^- anion. The π bonding between the Pb 6p orbitals and the B_8 motif can be seen clearly in HOMO – 1 ($6p_z$ – π bonding) and the degenerate HOMO ($6p_x/6p_y$ – π bonding). However, the coordination to Pb does not distort the planar B_8 framework significantly mainly due to the large size of the Pb atom and the relatively weak π bonding between the Pb atom and the B_8 motif. The degenerate LUMO (e_1) represents antibonding π interactions between the Pb $6p_x/6p_y$ orbitals and the π orbitals of the B_8 motif. Occupation of the LUMO by one electron gives rise to a 2E_1 degenerate electronic state under the C_{7v} symmetry, which is unstable due to the JT effect and will spontaneously distort to the lower C_s symmetry.

Conversely, removal of the SOMO electron in PbB_8^- (Figure 3) spontaneously restores the C_{7v} symmetry for the neutral PbB_8 borozene complex. What is surprising is the large change of the Pb position between the anion and the neutral. In the previous study on the LiB_8^- borozene complex [$Li^+(B_8^{2-})$],¹⁸ electron detachment from its HOMO (e_1), which is a degenerate π orbital on the B_8^{2-} borozene motif, also produces a 2E_1 degenerate electronic state under the C_{7v} symmetry. But the JT distortion is relatively small, judging from the observed photoelectron spectrum. In our very recent study of a similar CuB_8^- borozene complex [$Cu^+(B_8^{2-})$], negligible JT distortion is observed in the open-shell C_{7v} neutral CuB_8 (2E_1).²³

The large change of the Pb position in the PbB_8^- anion can be understood from the nature of the LUMO of PbB_8 , which involves antibonding π interactions between the Pb $6p_x/6p_y$ orbitals and the π orbitals of the B_8 motif. The large off-axis distortion of the Pb atom is to reduce the antibonding interaction, as shown more clearly in the SOMO of PbB_8^- (Figure 3). In fact, the SOMO of PbB_8^- even involves a slight bonding interaction because of the large shift of the Pb position to one side of the B_8 motif. Our preliminary calculation suggests that ionization of the SOMO electron in the C_s BiB_8 cluster will produce a closed-shell C_{7v} BiB_8^+

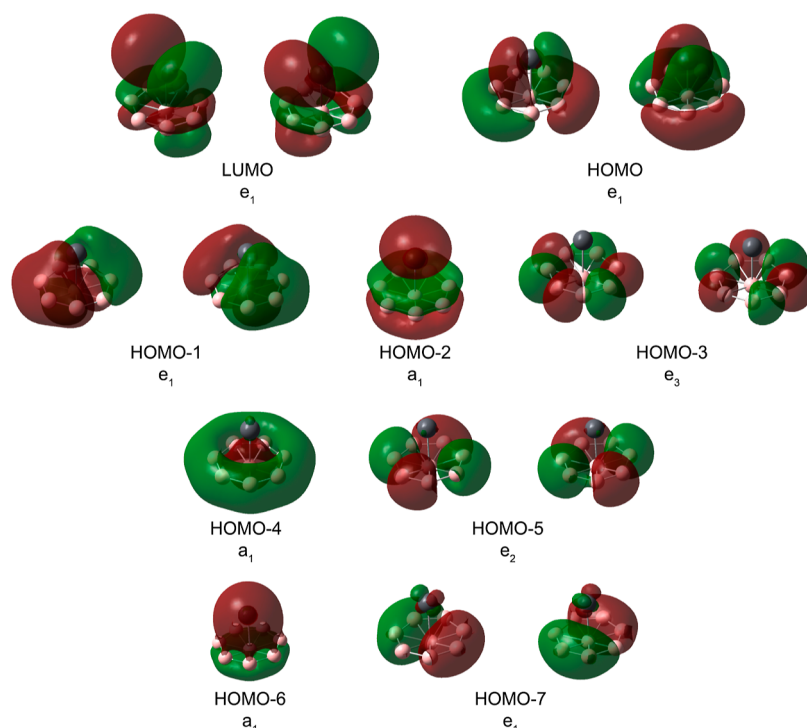


Figure 5. Valence MOs of the C_{7v} PbB_8 borozene complex.

cationic borozene complex, similar to the PbB_8 neutral borozene complex. Thus, the position of the large Bi or Pb atom on the surface of the B_8 borozene is controlled by the addition or removal of an electron, which can be viewed as a new type of molecular switches.⁵⁴

5. CONCLUSIONS

In conclusion, we report a PES and computational study of a new Pb-borozene complex, PbB_8^- . PES of PbB_8^- reveals a large geometry change upon electron detachment and a large HOMO–LUMO gap. Theoretical calculations find that neutral PbB_8 is a highly symmetric closed-shell Pb-borozene complex, C_{7v} $Pb^{2+}(B_8^{2-})$. The LUMO of PbB_8 is a degenerate π orbital involving antibonding interactions between the Pb $6p_x/6p_y$ orbitals and the π orbitals of the B_8 motif. Occupation of the degenerate LUMO induces a spontaneous symmetry-breaking due to the JT effect to yield a C_s PbB_8^- , in which the Pb atom is moved to one side of the B_8 borozene surface off the C_7 axis. The large change of the Pb position is a result of reducing the antibonding interaction between the Pb $6p$ orbital and the π orbital of the B_8 borozene in the anion. Thus, the position of the Pb atom on the surface of the B_8 borozene is controlled by the addition or removal of an electron, whereas there is relatively minor structural change of the B_8 motif between the PbB_8^- anion and the PbB_8 neutral borozene complex.

■ ASSOCIATED CONTENT

SI Supporting Information

The Supporting Information is available free of charge at <https://pubs.acs.org/doi/10.1021/acs.jpca.4c01282>.

Calculated VDEs for the low-lying isomer of PbB_8^- , comparison of the computed VDEs of the GM and low-lying isomer of PbB_8^- with the photoelectron spectrum, comparison of the Franck–Condon calculation with the

photoelectron spectrum, and Cartesian coordinates of the GM and low-lying isomers of PbB_8 and PbB_8^- (PDF)

■ AUTHOR INFORMATION

Corresponding Authors

Dao-Fu Yuan – Department of Chemistry, Brown University, Providence, Rhode Island 02912, United States; Hefei National Research Center for Physical Science at Microscale, University of Science and Technology of China, Hefei 230026, China; orcid.org/0000-0001-8461-6889; Email: ydfu@ustc.edu.cn

Lai-Sheng Wang – Department of Chemistry, Brown University, Providence, Rhode Island 02912, United States; orcid.org/0000-0003-1816-5738; Email: lai-sheng_wang@brown.edu

Authors

Wei-Jia Chen – Department of Chemistry, Brown University, Providence, Rhode Island 02912, United States

Hyun Wook Choi – Department of Chemistry, Brown University, Providence, Rhode Island 02912, United States

Joseph Cavanagh – Department of Chemistry, Brown University, Providence, Rhode Island 02912, United States

Complete contact information is available at: <https://pubs.acs.org/doi/10.1021/acs.jpca.4c01282>

Author Contributions

[§]W.-J. C. and H. W. C. contributed equally to this work.

Notes

The authors declare no competing financial interest.

■ ACKNOWLEDGMENTS

This work was supported by the National Science Foundation under Grant no. CHE-2403841 (to L.-S.W.). The calculation

was performed using computational resources and services provided by CCV of Brown University.

REFERENCES

- (1) Bersuker, I. B. Spontaneous symmetry breaking in matter induced by degeneracies and pseudodegeneracies. *Adv. Chem. Phys.* **2016**, *160*, 159–208.
- (2) Lipscomb, W. N. The boranes and their relatives. *Science* **1977**, *196*, 1047–1055.
- (3) Albert, B.; Hillebrecht, H. Boron: elementary challenge for experimenters and theoreticians. *Angew. Chem., Int. Ed.* **2009**, *48*, 8640–8668.
- (4) Oganov, A. R.; Chen, J.; Gatti, C.; Ma, Y.; Ma, Y.; Glass, C. W.; Liu, Z.; Yu, T.; Kurakevych, O. O.; Solozhenko, V. L. Ionic high-pressure form of elemental boron. *Nature* **2009**, *457*, 863–867.
- (5) Alexandrova, A. N.; Boldyrev, A. I.; Zhai, H.-J.; Wang, L. S. All-boron aromatic clusters as potential new inorganic ligands and building blocks in chemistry. *Coord. Chem. Rev.* **2006**, *250*, 2811–2866.
- (6) Oger, E.; Crawford, N. R. M.; Kelting, R.; Weis, P.; Kappes, M. M.; Ahlrichs, R. Boron cluster cations: transition from planar to cylindrical structures. *Angew. Chem., Int. Ed.* **2007**, *46*, 8503–8506.
- (7) Sergeeva, A. P.; Popov, I. A.; Piazza, Z. A.; Li, W.-L.; Romanescu, C.; Wang, L. S.; Boldyrev, A. I. Understanding boron through size-selected clusters: structure, chemical bonding, and fluxionality. *Acc. Chem. Res.* **2014**, *47*, 1349–1358.
- (8) Wang, L. S. Photoelectron spectroscopy of size-selected boron clusters: from planar structures to borophenes and borospherenes. *Int. Rev. Phys. Chem.* **2016**, *35*, 69–142.
- (9) Pan, S.; Barroso, J.; Jalife, S.; Heine, T.; Asmis, K. R.; Merino, G. Fluxional Boron Clusters: From Theory to Reality. *Acc. Chem. Res.* **2019**, *52*, 2732–2744.
- (10) Jian, T.; Chen, X.; Li, S.; Boldyrev, A. I.; Li, J.; Wang, L. S. Probing the structures and bonding of size-selected boron and doped-boron clusters. *Chem. Soc. Rev.* **2019**, *48*, 3550–3591.
- (11) Piazza, Z. A.; Hu, H.-S.; Li, W.-L.; Zhao, Y.-F.; Li, J.; Wang, L. S. Planar hexagonal B₃₆ as a potential basis for extended single-atom layer boron sheets. *Nat. Commun.* **2014**, *5*, 3113.
- (12) Li, W.-L.; Chen, Q.; Tian, W.-J.; Bai, H.; Zhao, Y.-F.; Hu, H.-S.; Li, J.; Zhai, H.-J.; Li, S.-D.; Wang, L. S. The B₃₃ cluster with a double-hexagonal vacancy: a new and more flexible structural motif for borophene. *J. Am. Chem. Soc.* **2014**, *136*, 12257–12260.
- (13) Mannix, A. J.; Zhou, X.-F.; Kiraly, B.; Wood, J. D.; Alducin, D.; Myers, B. D.; Liu, X.; Fisher, B. L.; Santiago, U.; Guest, J. R.; et al. Synthesis of borophenes: Anisotropic, two-dimensional boron polymorphs. *Science* **2015**, *350*, 1513–1516.
- (14) Feng, B.; Zhang, J.; Zhong, Q.; Li, W.; Li, S.; Li, H.; Cheng, P.; Meng, S.; Chen, L.; Wu, K. Experimental realization of two-dimensional boron sheets. *Nat. Chem.* **2016**, *8*, 563–568.
- (15) Alexandrova, A. N.; Boldyrev, A. I.; Zhai, H.-J.; Wang, L. S. Electronic structure, isomerism, and chemical bonding in B₇⁻ and B₇. *J. Phys. Chem. A* **2004**, *108*, 3509–3517.
- (16) Zhai, H.-J.; Alexandrova, A. N.; Birch, K. A.; Boldyrev, A. I.; Wang, L. S. Hepta- and Octacoordinate Boron in Molecular Wheels of Eight- and Nine-Atom Boron Clusters: Observation and Confirmation. *Angew. Chem., Int. Ed.* **2003**, *42*, 6004–6008.
- (17) Li, W.-L.; Chen, T.-T.; Chen, W.-J.; Li, J.; Wang, L. S. Monovalent lanthanide (I) in borozene complexes. *Nat. Commun.* **2021**, *12*, 6467.
- (18) Alexandrova, A. N.; Zhai, H.-J.; Wang, L. S.; Boldyrev, A. I. Molecular wheel B₈²⁻ as a new inorganic ligand. Photoelectron spectroscopy and ab initio characterization of LiB₈⁻. *Inorg. Chem.* **2004**, *43*, 3552–3554.
- (19) Galeev, T. R.; Romanescu, C.; Li, W.-L.; Wang, L. S.; Boldyrev, A. I. Valence isoelectronic substitution in the B₈⁻ and B₉⁻ molecular wheels by an Al dopant atom: Umbrella-like structures of AlB₇⁻ and AlB₈⁻. *J. Chem. Phys.* **2011**, *135*, 104301.
- (20) Kulichenko, M.; Chen, W.-J.; Choi, H. W.; Yuan, D.-F.; Boldyrev, A. I.; Wang, L. S. Probing copper-boron interactions in the Cu₂B₈⁻ bimetallic cluster. *J. Vac. Sci. Technol., A* **2022**, *40*, 042201.
- (21) Chen, W.-J.; Zhang, Y.-Y.; Li, W.-L.; Choi, H. W.; Li, J.; Wang, L. S. AuB₈⁻: an Au-borozene complex. *Chem. Commun.* **2022**, *58*, 3134–3137.
- (22) Chen, W.-J.; Kulichenko, M.; Choi, H. W.; Cavanagh, J.; Yuan, D.-F.; Boldyrev, A. I.; Wang, L. S. Photoelectron spectroscopy of size-selected bismuth-boron clusters: BiB_n⁻ (n = 6–8). *J. Phys. Chem. A* **2021**, *125*, 6751–6760.
- (23) Chen, W.-J.; Pozdeev, A. S.; Choi, H. W.; Boldyrev, A. I.; Yuan, D.-F.; Popov, I. A.; Wang, L. S. Searching for stable copper borozene complexes in CuB₇⁻ and CuB₈⁻. *Phys. Chem. Chem. Phys.* **2024**. in press
- (24) Barroso, J.; Pan, S.; Merino, G. Structural transformations in boron clusters induced by metal doping. *Chem. Soc. Rev.* **2022**, *51*, 1098–1123.
- (25) Liao, Y.; Cruz, C. L.; von Ragué Schleyer, P.; Chen, Z. Many M@B_n boron wheels are local, but not global minima. *Phys. Chem. Chem. Phys.* **2012**, *14*, 14898–14904.
- (26) Jia, J.; Ma, L.; Wang, J. F.; Wu, H. S. Structures and stabilities of ScB_n (n = 1–12) clusters: an ab initio investigation. *J. Mol. Model.* **2013**, *19*, 3255–3261.
- (27) Reber, A. C.; Khanna, S. N. Electronic structure, stability, and oxidation of boron-magnesium clusters and cluster solids. *J. Chem. Phys.* **2015**, *142*, 054304.
- (28) Zhao, R. N.; Yuan, Y.; Han, J. G. Geometries and electronic properties of transition metal hafnium-doped boron clusters: a computational investigation. *Polycyclic Aromat. Compd.* **2016**, *36*, 252–272.
- (29) Saha, P.; Rahane, A. B.; Kumar, V.; Sukumar, N. Analysis of the electron density features of small boron clusters and the effects of doping with C, P, Al, Si, and Zn: Magic B₇P and B₈Si clusters. *Phys. Scr.* **2016**, *91*, 053005.
- (30) Mai, D. T. T.; Duong, L. V.; Tai, T. B.; Nguyen, M. T. Electronic structure and thermochemical parameters of the silicon-doped boron clusters B_nSi, with n = 8–14, and their anions. *J. Phys. Chem. A* **2016**, *120*, 3623–3633.
- (31) Yu, R.; Barroso, J.; Wang, M. H.; Liang, W. Y.; Chen, C.; Zarate, X.; Orozco-Ic, M.; Cui, Z. H.; Merino, G. Structure and bonding of molecular stirrers with formula B₇M₂⁻ and B₈M₂ (M = Zn, Cd, Hg). *Phys. Chem. Chem. Phys.* **2020**, *22*, 12312–12320.
- (32) Feng, X.; Shi, D.; Jia, J.; Wang, C. Structural evolution and electronic properties of germanium-doped boron clusters and their anions: GeB_n^{0/-} (n = 6–20). *J. Nanopart. Res.* **2022**, *24*, 124.
- (33) Romanescu, C.; Galeev, T. R.; Li, W.-L.; Boldyrev, A. I.; Wang, L. S. Aromatic metal-centered monocyclic boron rings: Co@B₈⁻ and Ru@B₉⁻. *Angew. Chem., Int. Ed.* **2011**, *50*, 9334–9337.
- (34) Romanescu, C.; Galeev, T. R.; Sergeeva, A. P.; Li, W.-L.; Wang, L. S.; Boldyrev, A. I. Experimental and computational evidence of octa- and nona-coordinated planar iron-doped boron clusters: Fe@B₈⁻ and Fe@B₉⁻. *J. Organomet. Chem.* **2012**, *721*–*722*, 148–154.
- (35) Li, W.-L.; Ivanov, A. S.; Federič, J.; Romanescu, C.; Černušák, I.; Boldyrev, A. I.; Wang, L. S. On the way to the highest coordination number in the planar metal-centered aromatic Ta@B₁₀⁻ cluster: evolution of the structures of TaB_n⁻ (n = 3–8). *J. Chem. Phys.* **2013**, *139*, 104312.
- (36) Romanescu, C.; Galeev, T. R.; Li, W.-L.; Boldyrev, A. I.; Wang, L. S. Transition-metal-centered monocyclic boron wheel clusters (M@B_n): A new class of aromatic borometallic compounds. *Acc. Chem. Res.* **2013**, *46*, 350–358.
- (37) Chen, T.-T.; Li, W.-L.; Bai, H.; Chen, W.-J.; Dong, X.-R.; Li, J.; Wang, L. S. Re@B₈⁻ and Re@B₉⁻: new members of the transition-metal-centered borometallic molecular wheel family. *J. Phys. Chem. A* **2019**, *123*, 5317–5324.
- (38) Ito, K.; Pu, Z.; Li, Q. S.; Schleyer, P. v. R. Cyclic boron clusters enclosing planar hypercoordinate cobalt, iron, and nickel. *Inorg. Chem.* **2008**, *47*, 10906–10910.

- (39) Luo, Q. Boron rings containing planar octa- and enneacoordinate cobalt, iron and nickel metal elements. *Sci. China Ser. B: Chem.* **2008**, *51*, 607–613.
- (40) Pu, Z.; Ito, K.; Schleyer, P. v. R.; Li, Q.-S. Planar hepta-octona- and decacoordinate first row d-block metals enclosed by boron rings. *Inorg. Chem.* **2009**, *48*, 10679–10686.
- (41) Wu, X.; Wang, Y.; Zhao, X.; Zhou, S.; Li, S. D.; Chen, M.; Zhao, J. Transition metal-doped B_n ($n = 7–10$) clusters: confirmation of a circular disk Jellium model. *Eur. Phys. J. Plus* **2021**, *136*, 328.
- (42) Song, B.; Yang, L. M. Two-dimensional hypercoordinate chemistry: Challenges and prospects. *WIREs Comput. Mol. Sci.* **2024**, *14*, No. e1699.
- (43) Frisch, M. J.; Trucks, G. W.; Schlegel, H. B.; Scuseria, G. E.; Robb, M. A.; Cheeseman, J. R.; Scalmani, G.; Barone, V.; Mennucci, B.; Petersson, G. A.; et al. *Gaussian 09*; Gaussian Inc., 2009.
- (44) Tao, J.; Perdew, J. P.; Staroverov, V. N.; Scuseria, G. E. Climbing the density functional ladder: Nonempirical meta-generalized gradient approximation designed for molecules and solids. *Phys. Rev. Lett.* **2003**, *91*, 146401.
- (45) Peterson, K. A. Systematically convergent basis sets with relativistic pseudopotentials. I. Correlation consistent basis sets for the post-d group 13–15 elements. *J. Chem. Phys.* **2003**, *119*, 11099–11112.
- (46) Kendall, R. A.; Dunning, T. H.; Harrison, R. J. Electron affinities of the first-row atoms revisited. Systematic basis sets and wave functions. *J. Chem. Phys.* **1992**, *96*, 6796–6806.
- (47) Bauernschmitt, R.; Ahlrichs, R. Treatment of electronic excitations within the adiabatic approximation of time dependent density functional theory. *Chem. Phys. Lett.* **1996**, *256*, 454–464.
- (48) Bannwarth, C.; Grimme, S. A simplified time-dependent density functional theory approach for electronic ultraviolet and circular dichroism spectra of very large molecules. *Comput. Theor. Chem.* **2014**, *1040–1041*, 45–53.
- (49) Zubarev, D. Y.; Boldyrev, A. I. Developing paradigms of chemical bonding: adaptive natural density partitioning. *Phys. Chem. Chem. Phys.* **2008**, *10*, 5207–5217.
- (50) Zubarev, D. Y.; Boldyrev, A. I. Revealing intuitively assessable chemical bonding patterns in organic aromatic molecules via adaptive natural density partitioning. *J. Org. Chem.* **2008**, *73*, 9251–9258.
- (51) Lu, T.; Chen, F. Multiwfn: A multifunctional wavefunction analyzer. *J. Comput. Chem.* **2012**, *33*, 580–592.
- (52) Yuan, D. F.; Trabelsi, T.; Zhang, Y. R.; Francisco, J. S.; Wang, L. S. Probing the electronic structure and bond dissociation of SO_3 and SO_3^- using high-resolution cryogenic photoelectron imaging. *J. Am. Chem. Soc.* **2022**, *144*, 13740–13747.
- (53) Pyykko, P. Relativistic effects in structural chemistry. *Chem. Rev.* **1988**, *88*, 563–594.
- (54) Harris, J. D.; Moran, M. J.; Aprahamian, I. New molecular switch architectures. *Proc. Natl. Acad. Sci. U.S.A.* **2018**, *115*, 9414–9422.